JACS
JOURNAL OF THE AMERICAN CHEMICAL SOCIETY
Article
pubs.acs.org/JACS

Reduced and Superreduced Diplatinum Complexes

Tania V. Darnton,[†,⊥] Bryan M. Hunter,[†,⊥] Michael G. Hill,[‡] Stanislav Záliš,*[,§] Antonín Vlček Jr.,*[,§,∥] and Harry B. Gray*[,†]

[†]Beckman Institute, California Institute of Technology, Pasadena, California 91125, United States
[‡]Occidental College, Los Angeles, California 90041, United States
[§]J. Heyrovský Institute of Physical Chemistry, Czech Academy of Sciences, Dolejškova 3, CZ-182 23 Prague, Czech Republic
[∥]School of Biological and Chemical Sciences, Queen Mary University of London, Mile End Road, London E1 4NS, United Kingdom

Supporting Information

ABSTRACT: A d^8–d^8 complex $[Pt_2(\mu\text{-}P_2O_5(BF_2)_4]^{4-}$ (abbreviated $Pt(pop\text{-}BF_2)^{4-}$) undergoes two $1e^-$ reductions at $E_{1/2}$ = −1.68 and E_p = −2.46 V (vs Fc^+/Fc) producing reduced $Pt(pop\text{-}BF_2)^{5-}$ and superreduced $Pt(pop\text{-}BF_2)^{6-}$ species, respectively. The EPR spectrum of $Pt(pop\text{-}BF_2)^{5-}$ and UV–vis spectra of both the reduced and the superreduced complexes, together with TD-DFT calculations, reveal successive filling of the 6pσ orbital accompanied by gradual strengthening of Pt–Pt bonding interactions and, because of 6pσ delocalization, of Pt–P bonds in the course of the two reductions. Mayer–Millikan Pt–Pt bond orders of 0.173, 0.268, and 0.340 were calculated for the parent, reduced, and superreduced complexes, respectively. The second (5−/6−) reduction is accompanied by a structural distortion that is experimentally manifested by electrochemical irreversibility. Both reduction steps proceed without changing either d^8 Pt electronic configuration, making the superreduced $Pt(pop\text{-}BF_2)^{6-}$ a very rare $6p^2$ σ-bonded binuclear complex. However, the Pt–Pt σ bonding interaction is limited by the relatively long bridging-ligand-imposed Pt–Pt distance accompanied by repulsive electronic congestion. $Pt(pop\text{-}BF_2)^{4-}$ is predicted to be a very strong photooxidant (potentials of +1.57 and +0.86 V are estimated for the singlet and triplet dσ*pσ excited states, respectively).

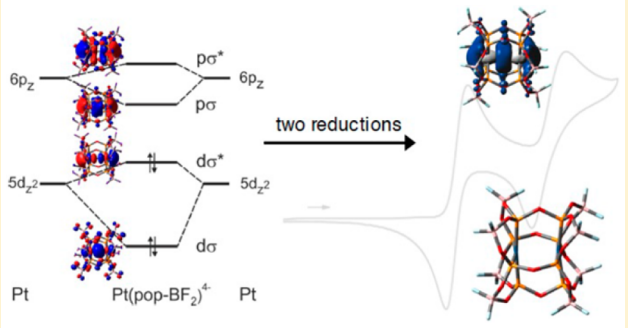

INTRODUCTION

The prototypal d^8–d^8 binuclear complex $Pt_2(P_2O_5H_2)_4^{4-}$ (abbreviated $Pt(pop)^{4-}$) and its perfluoroborated derivative $Pt_2(P_2O_5(BF_2)_2)_4^{4-}$ ($Pt(pop\text{-}BF_2)^{4-}$) have similar electronic structures and UV–vis absorption spectra, but profoundly different photophysics.[1−3] The HOMO is a Pt–Pt σ-antibonding orbital (dσ*); interestingly, the LUMO is Pt–Pt bonding (pσ), albeit ∼50% delocalized over the phosphorus ligands.[2] These two frontier orbitals are well separated from lower-lying occupied and higher unoccupied orbitals (Figure 1). In $Pt(pop\text{-}BF_2)^{4-}$, pairs of bridging ligands are covalently connected by BF_2 groups, forming a rigid cage around the photo- and electroactive Pt–Pt unit that features outward facing fluorine atoms. This extra rigidity and shielding likely are responsible for the dramatically enhanced lifetime of the lowest dσ* → pσ singlet excited state (1.6 ns vs ca. 3 ps for $Pt(pop)^{4-}$).[1,4] Electron excitation into the pσ orbital strengthens the Pt–Pt interaction, as evidenced by 0.18 Å bond shortening (calcd for $Pt(pop\text{-}BF_2)$;[2] 0.21–0.31 Å determined[5−8] by X-ray and optical techniques for Pt(pop)) and a 38–45 cm^{-1} increase of the Pt–Pt stretching frequency in both Pt(pop) and $Pt(pop\text{-}BF_2)$.[4,7−10] In analogy to optical excitation, reduction is expected to fill the pσ orbital, forming a weak Pt–Pt bond in $Pt(pop\text{-}BF_2)^{5-}$. Although reversible electrochemical reduction of $Pt(pop)^{4-}$ has not been reported,[11] $Pt(pop)^{5-}$ with a 34 μs lifetime was generated by pulse radiolysis in aqueous solution.[12] What is more, transient generation of a reduced species was indicated by observation of electrochemiluminescence at a platinum electrode in MeCN upon high-frequency potential switching.[13,14] As reducible –O–H···O– hydrogens are absent in $Pt(pop\text{-}BF_2)^{4-}$, we thought it likely that the complex could be reduced reversibly, and we have observed a two-step sequential reduction of $Pt(pop\text{-}BF_2)^{4-}$. The electronic structures of the two reduced forms have been investigated by DFT as well as spectroelectrochemical methods.

RESULTS

$Pt(pop\text{-}BF_2)^{4-}$ in MeCN at 273 K undergoes one-electron reductions at $E_{1/2}$ = −1.68 and E_p = −2.46 V vs Fc^+/Fc (Figure 2). The first wave is chemically reversible and electrochemically quasireversible at a scan rate of 50 mV/s (ΔE_p = 155 mV; as compared to ∼100 mV obtained for Fc^+/Fc under virtually identical conditions). The second wave is electrochemically irreversible and chemically reversible, indicating formation of a

Received: March 9, 2016
Published: April 11, 2016

ACS Publications © 2016 American Chemical Society

DOI: 10.1021/jacs.6b02559
J. Am. Chem. Soc. 2016, 138, 5699–5705

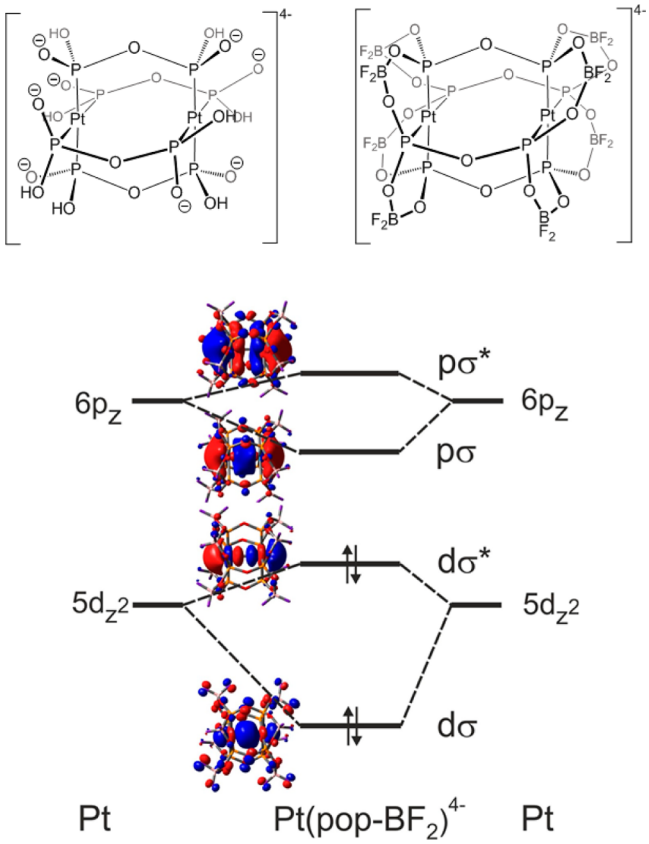

Figure 1. Structural representations of Pt(pop)$^{4-}$ and Pt(pop-BF$_2$)$^{4-}$ along with a qualitative σ-MO scheme.

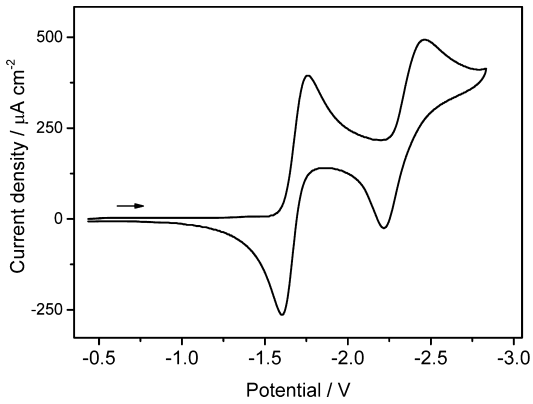

Figure 2. Cyclic voltammogram of Pt(pop-BF$_2$)$^{4-}$ in MeCN containing 0.1 M Bu$_4$NPF$_6$ at 273 K. Potentials vs Fc+/Fc. Scan rate 50 mV/s.

superreduced complex Pt(pop-BF$_2$)$^{6-}$, stable at least at 273 K. At room temperature, the peak-current ratio of the second wave is less than unity and two small shoulders appear at its positive site, attributable to decomposition products (Figure S1). Scanning over the anodic region (Figure S2) reveals a 2-electron chemically irreversible oxidation at +0.94 V (vs Fc$^+$/Fc).

UV−vis spectroelectrochemistry in MeCN at 273 K carried out at the potential of the first reduction wave shows a decrease in intensity of the 365 nm band of Pt(pop-BF$_2$)$^{4-}$ accompanied by a rise of a sharp band at 416 nm with shoulders at ca. 411 and ∼450 nm, and broad weak bands at ∼550 and 338 nm, all attributable to Pt(pop-BF$_2$)$^{5-}$ (Figure 3). The parent complex

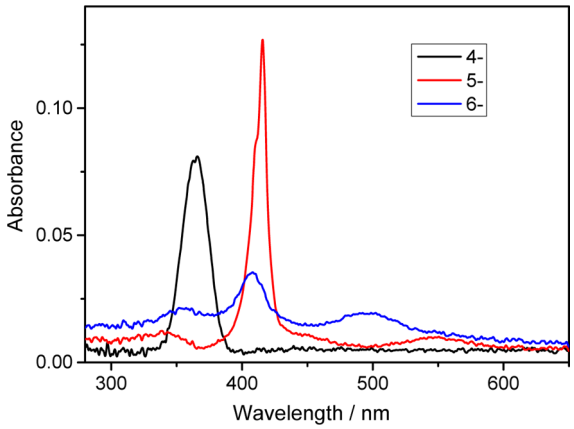

Figure 3. UV−vis absorption spectra of Pt(pop-BF$_2$)$^{4-}$ (black) and in situ spectroelectrochemically produced Pt(pop-BF$_2$)$^{5-}$ (red) and Pt(pop-BF$_2$)$^{6-}$ (blue, contains ca. 20% of Pt(pop-BF$_2$)$^{5-}$). Conditions: glassy carbon working electrode, MeCN, 0.1 M Bu$_4$NPF$_6$, 273 K. Binomial smoothing applied. Spectra measured in the course of reduction and subsequent reoxidation are shown in Figures S3 and S4.

is nearly quantitatively recovered upon anodically switching the potential (Figure S3). Further reduction at more negative potentials yields a spectrum with three distinct features (356, 408, and 496 nm; Figure 3). Spectra measured in the course of the second reduction (Figure S4) show an isosbestic point, indicating conversion to the superreduced species Pt(pop-BF$_2$)$^{6-}$. Reoxidation at more positive potentials initially recovers Pt(pop-BF$_2$)$^{5-}$ at 273 K (Figure S4), whereas an unidentified species strongly absorbing at 350 nm is formed at room temperature. Experimental spectra of both the reduced and the superreduced species match those calculated by TD-DFT (Figure S5), supporting their assignments as Pt(pop-BF$_2$)$^{5-}$ and Pt(pop-BF$_2$)$^{6-}$, respectively.

The reduced species Pt(pop-BF$_2$)$^{5-}$ also was characterized by EPR, after reduction with Na/Hg and freezing to 77 K. Both experimental and simulated spectra are shown in Figure 4 (parameters are given in Table S1). The EPR spectrum is characteristic of a spin-doublet state with an axial spin distribution ($g_2 \cong g_3 \neq g_1$). Hyperfine splitting constants due to the two ^{195}Pt nuclei are similar, indicating a nearly symmetrical spin density distribution. The g values are similar to those determined for Pt(II) complexes with radical-anion ligands.[15,16] In contrast, "platinum blue" species, where the unpaired electron is delocalized over four Pt atoms in a molecular orbital with predominantly 5d-character, also exhibit axial EPR spectra but with much larger g values as well as pronounced anisotropy.[17,18] Still larger g values have been reported for Pt(I) d^9 sites.[19] The EPR data for Pt(pop-BF$_2$)$^{5-}$ suggest that the unpaired electron is delocalized over the two Pt atoms as well as the ligands in a molecular orbital of 6p-character. Our interpretation is supported by DFT spin-density calculations (Figure 5), which accurately reproduce the g values (Table S1).

Molecular and Electronic Structures: DFT Calculations. DFT optimizations of the reduced and superreduced species in MeCN were performed without symmetry constraints. Calculations started from several different initial structures, including asymmetric ones, to ensure that the absolute energy minimum was found. Structural optimization shows successive Pt−Pt and Pt−P bond shortening upon each one-electron reduction (Tables 1 and S2). The P$_4$Pt units,

DOI: 10.1021/jacs.6b02559
J. Am. Chem. Soc. 2016, 138, 5699−5705

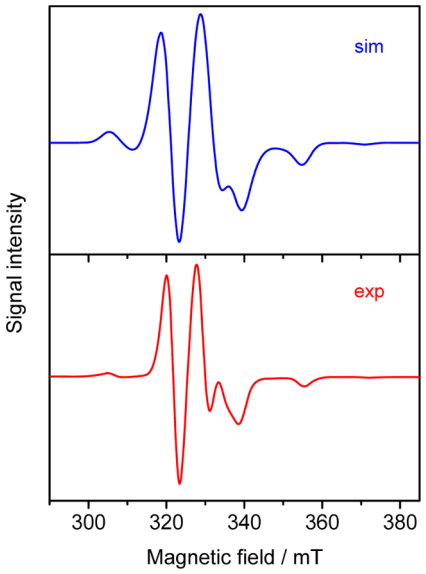

Figure 4. Experimental (bottom) and simulated (top) EPR spectra of $Pt(pop\text{-}BF_2)^{5-}$ obtained after $Pt(pop\text{-}BF_2)^{4-}$ reduction with Na/Hg in MeCN at room temperature. Simulated parameters: g_1 = 1.98, g_2 = 2.03, g_3 = 2.04; A(Pt) = 550, 550, 900 MHz; A(Pt′) = 350, 500, 900 MHz.

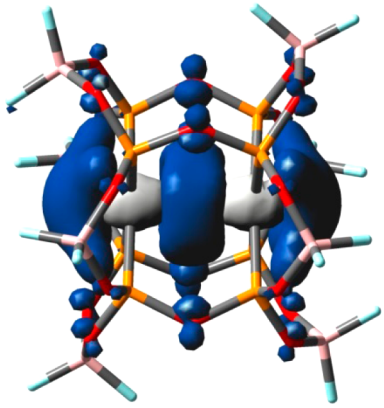

Figure 5. DFT(PBE0/PCM-MeCN) calculated spin-density distribution in $Pt(pop\text{-}BF_2)^{5-}$ in MeCN solution.

which are almost planar in $Pt(pop\text{-}BF_2)^{4-}$, bend slightly outward upon the first reduction. The two platinum atoms remain approximately equivalent, as evidenced by nearly identical Pt(1)−P and Pt(2)−P distances (Table S1). The inclusion of five Me_4N^+ cations in the calculation did not change the symmetrical molecular structure of $Pt(pop\text{-}BF_2)^{5-}$, although the cations adopted an asymmetric distribution around the 5− anion.

Two stable structures were calculated for superreduced $Pt(pop\text{-}BF_2)^{6-}$. The slightly asymmetric conformation (denoted **6**) is the more stable one with small angular distortions around the Pt atoms (Tables 1, S2, and Figure S6). The other calculated conformation (**6′**) is nearly symmetrical, much like the 5− species, with the Pt atoms displaced inward with respect to the surrounding P_4 planes. The calculated free energy of **6′** is 0.096 eV higher than that of **6**, and the Pt−Pt and Pt−P bonds are shorter relative to $Pt(pop\text{-}BF_2)^{5-}$ in both conformations. Structural optimization in the presence of six Me_4N^+ cations yields a structure similar to **6**, with an asymmetrical distribution of cations (Figure S7).

The two reduction steps correspond to successive filling of the pσ orbital (Figure 1), whose calculated Pt character increases from 43% in the parent complex to about 59% in both the 5− and 6− species. Accordingly, the calculated spin density in $Pt(pop\text{-}BF_2)^{5-}$ is nearly symmetrically distributed between and around the two Pt atoms (Figure 5, Table S1). The strong narrow band in the $Pt(pop\text{-}BF_2)^{5-}$ UV−vis absorption spectrum is due to a transition of predominantly βHOMO → βLUMO (dσ* → pσ) character (Table 2, Figure 6); it is red-shifted relative to the corresponding band of the parent complex (416 vs 365 nm[1]), but of comparable integrated intensity (Figures 3 and S3). The high-energy shoulder is attributable to vibronic structure: corresponding peak wavenumbers of 24 050 and 24 380 cm^{-1}, separated by 330 cm^{-1}, were obtained by Gaussian decomposition. (The absorption

Table 2. TD-DFT (PBE0/PCM-MeCN) Calculated Lowest Doublet Excitation Energies for $Pt(pop\text{-}BF_2)^{5-}$[a]

state	main contributing excitations (%)	transition energy, eV (nm)	oscillator strength	exptl. eV, nm
b^2A	99 (αHOMO → αLUMO+1)	2.32 (533)	0.0[b]	
c^2A	70 (αHOMO → αLUMO)	2.43 (509)	0.036	∼550
	23 (βHOMO → βLUMO)			
d^2A	99 (αHOMO → αLUMO+2)	2.46 (505)	0.0[b]	∼450
e^2A	74 (βHOMO → βLUMO)	3.02 (411)	0.285	416
	25 (αHOMO → αLUMO)			
f^2A	90 (αHOMO → αLUMO+6)	3.82 (325)	0.009	338
g^2A	99 (αHOMO → αLUMO+7)	3.82 (325)	0.015	

[a]The MOs (spin-orbitals) involved in the lowest excitations are depicted in Figure 6; αLUMO+6 and αLUMO+7 are mostly localized on $pop\text{-}BF_2$. [b]Oscillator strengths become nonzero ($\sim 2 \times 10^{-4}$) when spin−orbit coupling is approximately included.

Table 1. Selected Bond Lengths (Å) of $Pt(pop\text{-}BF_2)^{n-}$ (n = 4, 5, 6) Calculated by DFT(PBE0/PCM-MeCN)

	n =						
	4	5	Δ(5−4)	6	Δ(6−5)	6′	Δ(6′−5)
Pt−Pt	2.887	2.803	−0.084	2.739	−0.058	2.745	−0.058
Pt−P (average)	2.301	2.278	−0.025	2.255	−0.023	2.255	−0.023
P−O(−P) (average)	1.625	1.634	0.009	1.643	0.010	1.644	0.010
P−Pt−P (average)	178.8[a]	177.1[a]	−1.7	166.8,[a] −175.7[b]	−10.3 7.2	176.0[a]	−1.1

[a]The P → Pt vectors point inward to the Pt−Pt unit. [b]The P → Pt vectors point outward from the Pt−Pt unit. The Pt−P directions are reversed at the other PtP_4 unit (Figure S4, Table S1).

DOI: 10.1021/jacs.6b02559
J. Am. Chem. Soc. 2016, 138, 5699−5705

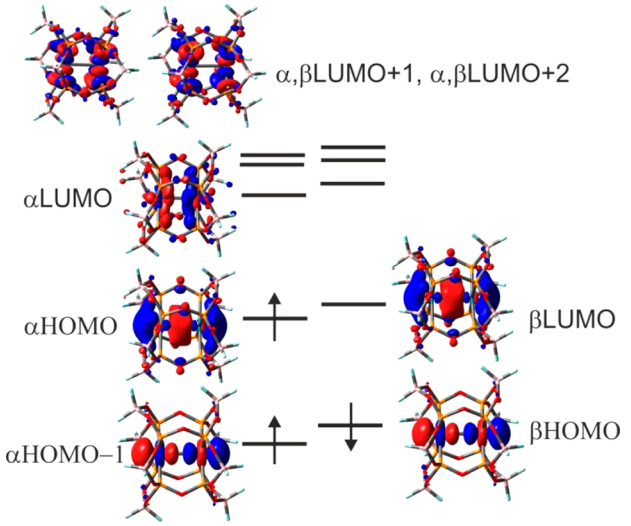

Figure 6. Frontier molecular orbitals (spin-orbitals) involved in the lowest electronic transitions of $Pt(pop\text{-}BF_2)^{5-}$.

band can be decomposed into four Gaussians with an average separation of 270 cm^{-1}.) Several mixed $\delta(POP)/\nu(PtPt)$ vibrations are expected[4] to occur in this frequency range. The lowest absorption band (550 nm) of $Pt(pop\text{-}BF_2)^{5-}$ has no counterpart in the $Pt(pop\text{-}BF_2)^{4-}$ spectrum. The transition in question predominantly involves excitation from a pσ orbital (αHOMO) to a ligand-localized molecular orbital that also contains a dσ* admixture (αLUMO). This transition gains intensity from the 23% contribution of βHOMO → βLUMO (dσ* → pσ) excitation (Table 2).

The doubly occupied pσ HOMO in the superreduced species **6** is polarized toward one of the Pt atoms (Figure 7), making

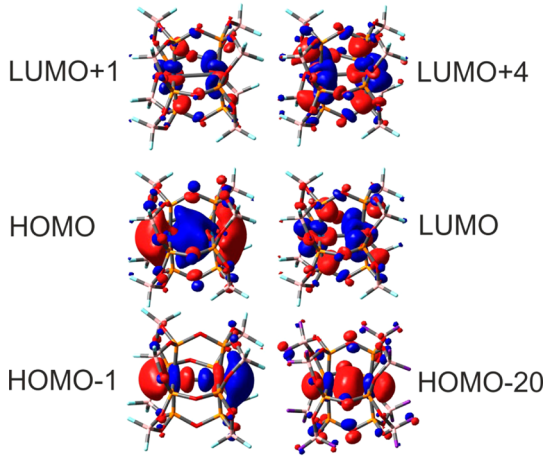

Figure 7. Frontier molecular orbitals involved in the lowest electronic transitions of $Pt(pop\text{-}BF_2)^{6-}$/conformer **6**. HOMO is the 6pσ orbital; HOMO−1 and HOMO−20 are the 5dσ* and 5dσ orbitals, respectively.

the electron distribution slightly asymmetric. Each Pt atom in **6** formally keeps its $5d^8$ electron configuration, while the two Pt atoms are connected by a 2-electron σ-bond arising from $6p_z$–$6p_z$ orbital overlap. With a $(d\sigma^*)^2(p\sigma)^2$ configuration, spectroscopically relevant electronic transitions are unrelated to those of the parent complex. These transitions, which originate from the pσ HOMO, are directed into higher unoccupied orbitals of mixed metal/ligand character (Table 3). The lowest broad band due to the HOMO → LUMO transition involves a small electron-density shift between the Pt atoms; the transition weakens the Pt–Pt bond because of both HOMO(pσ) depopulation and the partial pσ* character of the LUMO. The absorption spectrum calculated for the more symmetrical configuration **6′** shows only one principal band (Table S3, Figure S8). It is very different from both the experimental spectrum and the spectrum calculated for **6** (Figure S5a).

Table 3. TD-DFT (PBE0/PCM-MeCN) Calculated Lowest Singlet Excitation Energies (eV) for $Pt(pop\text{-}BF_2)^{6-}$/Conformation 6[a]

state	main contributing excitations (%)	transition energy eV (nm)	oscillator strength	exptl. (nm)
b^1A	90 (HOMO → LUMO)	2.53 (490)	0.184	496
c^1A	80 (HOMO → LUMO +1)	3.07 (404)	0.075	408
	10 (HOMO → LUMO +4)			
d^1A	87 (HOMO → LUMO +4)	3.53 (350)	0.081	356
	12 (HOMO → LUMO +1)			
e^1A	92 (HOMO → LUMO +6)	4.00 (310)	0.016	
f^1A	70 (HOMO → LUMO +7)	4.08 (304)	0.013	

[a]The relevant MOs are depicted in Figure 7.

DISCUSSION

Perfluoroboration strongly stabilizes reduced forms of $Pt(pop)^{4-}$. The reduced $Pt(pop\text{-}BF_2)^{5-}$ and superreduced $Pt(pop\text{-}BF_2)^{6-}$ are stable in MeCN solution at least on the order of minutes, as compared to microsecond–millisecond times[12,13] in the case of $Pt(pop)^{5-}$ (and it is not likely that $Pt(pop)^{6-}$ can be isolated[20]). The enhanced stability of the reduced and superreduced forms is attributable to the lack of reducible hydrogen atoms in the covalently linked inorganic cage around the Pt–Pt unit. The large potential difference (~0.7 V) between the first and second reductions indicates that disproportionation of $Pt(pop\text{-}BF_2)^{5-}$ is disfavored.

The first reduction of $Pt(pop\text{-}BF_2)^{4-}$ occurs at −1.68 V (vs Fc^+/Fc), as compared to ca. −1.8 V for Pt(pop). (The Pt(pop) value was estimated[21] from excited-state reductive quenching kinetics in MeOH. No electrochemical reduction wave was reported.) This redox-potential difference is attributable to the electron-withdrawing effect of BF_2, transmitted to the Pt–Pt unit by pσ delocalization over the P donor atoms (Figures 1, 6, and 7). It follows that electronically excited $Pt(pop\text{-}BF_2)^{4-}$ is a very strong oxidant: potentials of +1.57 and +0.86 V (vs Fc^+/Fc) can be estimated for $*^1Pt(pop\text{-}BF_2)^{4-/5-}$ and $*^3Pt(pop\text{-}BF_2)^{4-/5-}$ redox couples, respectively (using spectroscopically determined excited-state energies[4]). In comparison, the $*^3Pt(pop)^{4-/5-}$ couple is estimated to be +0.7 V.[21] Because of the stability of the reduced species and the shielding effect of the eight BF_2 groups, reductive quenching of excited $Pt(pop\text{-}BF_2)^{4-}$ should be reversible and occur with a high cage-escape yield (80% was reported[21] for quenching of $*^3Pt(pop)$ by dimethylaniline). $Pt(pop\text{-}BF_2)^{4-}$ thus emerges as a promising

DOI: 10.1021/jacs.6b02559
J. Am. Chem. Soc. 2016, 138, 5699–5705

photooxidant that could be employed to drive steps in organic reactions.

The reduced species $Pt(pop\text{-}BF_2)^{5-}$ can be generated by electrochemical or chemical reduction and also by irradiating the parent complex in the presence of an irreversible reductive quencher.[22] It could reduce substrates in reactions involving both outer- and inner-sphere activation. However, the radical-like reactivity typical for $^{*3}Pt(pop)^{23-25}$ is not expected for the reduced species, because the outward-oriented $d\sigma^*$ orbital is doubly occupied, unlike the excited state. The superreduced $Pt(pop\text{-}BF_2)^{6-}$ can only be produced electrochemically or by using very strong chemical reductants. In a preliminary experiment, we found $Pt(pop\text{-}BF_2)^{6-}$ to be much more reactive toward CH_2Cl_2 than $Pt(pop\text{-}BF_2)^{5-}$ (Figure S9). Rates of outer-sphere electron transfer reactions of $Pt(pop\text{-}BF_2)^{6-}$ will be limited by large reorganization energies, as indicated by the electrochemical irreversibility of the 5−/6− CV wave at the 50 mV/s scan rate (Figure 2). The relatively slow second reduction step correlates with increasing structural reorganization, as revealed by DFT (Tables 1 and S2, Figure S6).

Spectroscopic changes recorded in the course of the reduction together with DFT calculations point to successive filling of the $p\sigma$ molecular orbital: The strong, sharp $d\sigma^*\rightarrow p\sigma$ band is the lowest-energy feature in the spectrum of the parent complex. It also is present in the reduced (5−) species with a $(d\sigma^*)^2(p\sigma)^1$ configuration but preceded in energy by a weaker band attributable to $p\sigma$ excitation (Table 2). The UV−vis spectral pattern changes completely in the superreduced complex, as the $p\sigma$ orbital becomes fully occupied. The $d\sigma^*\rightarrow p\sigma$ transition vanishes, and the spectrum exhibits a series of transitions from the $p\sigma$ HOMO to higher unoccupied orbitals (Table 3).

Successive filling of the $p\sigma$ orbital formally generates a Pt−Pt σ bond without changing the Pt $5d^8$ electronic configuration, making $Pt(pop\text{-}BF_2)^{6-}$ a very rare $6p^2$ σ-bonded binuclear complex. The DFT-calculated Mayer−Mulliken bond orders[26] show strengthening of the Pt−Pt bonding interaction upon reduction (Table 4), whereby the bond order increases about 2-fold on going from the 4− parent (0.17) to the 6− superreduced complex (0.34). While significant, the Pt−Pt bonding in $Pt(pop\text{-}BF_2)^{6-}$ is far from a full σ-bond. The Pt−Pt bonding interaction is limited by several structural and electronic factors: the rigid pop-BF_2 ligand cage does not allow the metal−metal distance to shorten very much, disfavoring effective orbital overlap; the $(5d\sigma)^2(5d\sigma^*)^2(6p\sigma)^2$ configuration places six σ electrons in spatial proximity with one another, producing repulsive electronic congestion along the Pt−Pt axis; and the $p\sigma$ molecular orbital is only 59% $6p_z$ in character, being delocalized over the Pt−P bonds (Figures 1, 6, and 7). Accordingly, Pt−P bond orders also gradually increase upon reduction (Table 4). The EPR spectrum of $Pt(pop\text{-}BF_2)^{5-}$ confirms the delocalized nature of the singly occupied $6p\sigma$ molecular orbital, showing axial spin density distribution.

Table 4. DFT-Calculated Mayer−Mulliken Bond Orders for $Pt(pop\text{-}BF_2)^{n-}$ Complexes[a]

	n		
bond	4	5	6/conf. **6**
Pt−Pt	0.173	0.268	0.340
Pt−P1	1.119	1.181	1.175
Pt−P2	1.122	1.173	1.309
Pt−P3	1.122	1.173	1.167
Pt−P4	1.119	1.182	1.312
Pt−P5	1.119	1.183	1.320
Pt−P6	1.121	1.174	1.175
Pt−P7	1.121	1.175	1.328
Pt−P8	1.119	1.183	1.168

[a]Atom P5 is in alignment with atom P1, etc.

The Pt−Pt distance was calculated to shorten by 0.08 and 0.06 Å upon the first and second reductions, respectively, while the calculated Pt−Pt stretching frequency ν(Pt−Pt) increases from 128 cm^{-1} in the parent complex to 146 (5−) and 170 cm^{-1} (6−). The reduced species essentially keeps the high symmetry of the parent complex, which is manifested both by the calculation (Table S2) and by the EPR spectrum. The most stable conformer of $Pt(pop\text{-}BF_2)^{6-}$ shows a small asymmetry, both between the two Pt centers and within each PtP_4 unit, where one pair of *trans* Pt−P bonds is shorter than the other. The HOMO also is distributed slightly asymmetrically, perhaps due to the "frustrated" $p\sigma$ interaction mentioned above. Nevertheless, the calculated natural charges at the two Pt atoms differ by only 0.035 e^-, in accordance with the $(5d\sigma)^2(5d\sigma^*)^2(6p\sigma)^2$ configuration. This behavior contrasts with that of doubly reduced $5d^8$-$5d^8$ $Ir_2(dimen)_4^{2+}$ (dimen =1,8-diisocyano-*p*-menthane) that adopts a d^8−d^{10} (Ir^{II}−Ir^0) mixed-valence configuration. In this case, one iridium center maintains a square planar local geometry, while the other distorts toward tetrahedral.[27] Such a distortion avoids the congested $(5d\sigma)^2(5d\sigma^*)^2(6p\sigma)^2$ electronic structure, and its stabilizing effect is manifested by the much smaller difference between the first and second reduction potentials of $Ir_2(dimen)_4^{2+}$ (0.19 V),[27] as compared to $Pt(pop\text{-}BF_2)$ (~0.7 V). Such a distortion toward a mixed-valence structure is possible in the $Ir_2(dimen)_4^{2+}$ case because of the structural flexibility of the dimen bridge,[28] whereas the rigid pop-BF_2 ligand cage of $Pt(pop\text{-}BF_2)^{6-}$ enforces a nearly symmetrical structure, producing the unusual partial $6p\sigma$ metal−metal bond. We plan to map the reactivity patterns of this powerful $(6p)^2$ σ-bond reductant.

EXPERIMENTAL SECTION

Materials and Procedures. $[Bu_4N]_4[Pt_2(P_2O_5(BF_2)_2)_4]$ was prepared as described previously.[1,22] All measurements were performed under an argon atmosphere in dry, degassed acetonitrile (HPLC grade, Fisher) that was passed through a solvent purification column. Bu_4NPF_6 (Fluka) was used as received. Electrolyte solutions were prepared and stored over activated alumina and 4-Å molecular sieves.

All electrochemical experiments were performed with a CH Instruments model 650A electrochemical analyzer. Cyclic voltammetry (CV) at ambient temperature was measured in a three-electrode configuration consisting of a highly polished glassy-carbon-disk working electrode (A = 0.07 cm^2), a Pt wire auxiliary electrode, and a 1.0 M KCl AgCl/Ag reference electrode, separated by a modified Luggin capillary. Low temperature CV was carried out using a nonisothermal cell configuration, in which the reference electrode was held at ambient temperature, separated from the working compartment by a long glass tube filled with electrolyte, and connected by a Luggin capillary. The temperature was monitored by a thermocouple placed in the working compartment. The ferrocenium/ferrocene couple has $E^{0\prime}$ = 0.434 V, measured at identical experimental conditions. All potentials in the text are reported vs Fc^+/Fc.

Thin-layer spectroelectrochemistry was carried out in a specular-reflectance mode using a modified IR cell. An Ocean Optics UV−vis light source (DH-2000) and spectrometer (USB2000) were connected to the Y-arms of a bifurcated fiber-optic cable; the end of the cable was

DOI: 10.1021/jacs.6b02559
J. Am. Chem. Soc. 2016, 138, 5699−5705

connected through a lens housing containing a semispherical collimating lens to the front-face window of the spectroelectrochemical cell at a 90° angle. A drop of mineral oil between the fiber optic and front-face quartz window of the cell ensures refractive-index matching. Spectra were not corrected for front-face reflection. The error in intensity at an absorbance of 0.5 is less than 1%. The glassy-carbon working electrode of the spectroelectrochemical cell was attached with silver epoxy to a brass cooling tube, connected to a circulating variable-temperature bath.

EPR spectra were recorded on a Bruker EMS spectrometer at 9.39 GHz. Samples at ∼10 mM concentration were prepared by reduction with Na/Hg in dry acetonitrile under an N_2 atmosphere and frozen with liquid nitrogen prior to the measurements. Spectral simulations were performed with MATLAB using the EasySpin MATLAB toolbox (version 4.5.5). Simulation parameters obtained include: g = [2.04, 2.03, 1.98]; HStrain = [180, 120, 100] MHz; A_{Pt1} = [550, 550, 900] MHz; A_{Pt2} = [350, 500, 900] MHz.

DFT Calculations. Electronic structures of $Pt(pop\text{-}BF_2)^{n-}$ (n = 4, 5, 6) complexes were calculated by density functional theory (DFT) methods using Gaussian 09[29] (G09) and ADF 2014.06[30] program packages. All calculations employed the hybrid Perdew, Burke, and Ernzerhof[31,32] (PBE0) exchange and correlation functional. The following basis sets were used within G09:6-311g(3d) polarized triple-ζ basis sets[33] for P and O: 6-31g(d) double-ζ for remaining first row atoms, and quasi-relativistic small-core effective core pseudopotentials and the corresponding optimized set of basis functions for Pt.[34,35] Mayer−Mulliken bond orders and natural charges were calculated by the NBO 6.0 program.[36]

The solvent was included using the polarizable calculation model (PCM).[37] Geometry optimizations, which were performed without any symmetry constraints, included the PCM solvent correction.[37] They were followed by vibrational analysis: no imaginary frequencies were found for energy minima. Open-shell systems were treated by the unrestricted Kohn−Sham (UKS) procedure. For comparison of spectra in different redox states, Me_4N^+ counterions corresponding to the negative charge of the complex anion were added. ADF calculations employed Slater-type orbital (STO) basis sets of triple-ζ quality with two polarization functions for the Pt atom, triple-ζ with polarization functions for O, P, and H atoms, and double-ζ with one polarization function for the remaining atoms. The basis set was represented by a frozen core approximation (1s for B, N, O, 1s−2p for P, and 1s−4d for Pt were kept frozen). The scalar relativistic (SR) zero-order regular approximation (ZORA) was used. Solvent effect corrections were calculated using the COSMO model.[38] The g tensor was obtained from a spin-nonpolarized wave function after incorporating spin−orbit (SO) coupling.[39] EPR parameters were calculated by single point procedures at optimized structures.

■ ASSOCIATED CONTENT

Supporting Information

The Supporting Information is available free of charge on the ACS Publications website at DOI: 10.1021/jacs.6b02559.

Room-temperature cyclic voltammetry, spectra monitored in the course of both reductions and respective reoxidations, TD-DFT simulated spectra, DFT calculated structures, and EPR parameters (PDF)

■ AUTHOR INFORMATION

Corresponding Authors

*zalis@jh-inst.cas.cz
*a.vlcek@qmul.ac.uk
*hbgray@caltech.edu

Author Contributions

⊥T.V.D. and B.M.H. contributed equally.

Notes

The authors declare no competing financial interest.

■ ACKNOWLEDGMENTS

We thank James Blakemore, Angelo Di Bilio, Yan-Choi Lam, and Jay R. Winkler for assistance with experiments and helpful discussions. This work was supported by the NSF CCI Solar Fuels Program (CHE-1305124). Additional support was provided by the Arnold and Mabel Beckman Foundation, the Ministry of Education of the Czech Republic (grants LH13015 and LD14129), and COST Actions CM1202 and CM1405. B.M.H. is a Fellow of the Resnick Sustainability Institute at Caltech; T.V.D. is an NSF Graduate Research Fellow.

■ REFERENCES

(1) Durrell, A. C.; Keller, G. E.; Lam, Y.-C.; Sýkora, J.; Vlček, A., Jr.; Gray, H. B. *J. Am. Chem. Soc.* **2012**, *134*, 14201−14207.
(2) Záliš, S.; Lam, Y. C.; Gray, H. B.; Vlček, A., Jr. *Inorg. Chem.* **2015**, *54*, 3491−3500.
(3) Roundhill, D. M.; Gray, H. B.; Che, C.-M. *Acc. Chem. Res.* **1989**, *22*, 55−61.
(4) Hofbeck, T.; Lam, Y. C.; Kalbáč, M.; Záliš, S.; Vlček, A.; Yersin, H. *Inorg. Chem.* **2016**, *55*, 2441−2449.
(5) van der Veen, R. M.; Milne, C. J.; El Nahhas, A.; Lima, F. A.; Pham, V.-T.; Best, J.; Weinstein, J. A.; Borca, C. N.; Abela, R.; Bressler, C.; Chergui, M. *Angew. Chem., Int. Ed.* **2009**, *48*, 2711−2714.
(6) Christensen, M.; Haldrup, K.; Bechgaard, K.; Feidenhans'l, R.; Kong, Q.; Cammarata, M.; Lo Russo, M.; Wulff, M.; Harrit, N.; N, M. M. *J. Am. Chem. Soc.* **2009**, *131*, 502−508.
(7) Rice, S. F.; Gray, H. B. *J. Am. Chem. Soc.* **1983**, *105*, 4571−4575.
(8) Che, C.-M.; Butler, L. G.; Gray, H. B.; Crooks, R. M.; Woodruff, W. H. *J. Am. Chem. Soc.* **1983**, *105*, 5492−5494.
(9) Stiegman, A. E.; Rice, S. F.; Gray, H. B.; Miskowski, V. M. *Inorg. Chem.* **1987**, *26*, 1112−1116.
(10) Fordyce, W. A.; Brummer, J. G.; Crosby, G. A. *J. Am. Chem. Soc.* **1981**, *103*, 7061−7064.
(11) Bryan, S. A.; Schmehl, R. H.; Roundhill, D. M. *J. Am. Chem. Soc.* **1986**, *108*, 5408−5412.
(12) Che, C.-M.; Atherton, S. J.; Butler, L. G.; Gray, H. B. *J. Am. Chem. Soc.* **1984**, *106*, 5143−5145.
(13) Vogler, A.; Kunkely, H. *Angew. Chem., Int. Ed. Engl.* **1984**, *23*, 316−317.
(14) Kim, J.; Fan, F. F.; Bard, A. J.; Che, C.-M.; Gray, H. B. *Chem. Phys. Lett.* **1985**, *121*, 543−546.
(15) Braterman, P. S.; Song, J.-I.; Vogler, C.; Kaim, W. *Inorg. Chem.* **1992**, *31*, 222−224.
(16) Hirani, B.; Li, J.; Djurovich, P. I.; Yousufuddin, M.; Oxgaard, J.; Persson, P.; Wilson, S. R.; Bau, R.; Goddard, W. A., III; Thompson, M. E. *Inorg. Chem.* **2007**, *46*, 3865−3875.
(17) Matsunami, J.; Urata, H.; Matsumoto, K. *Inorg. Chem.* **1995**, *34*, 202−208.
(18) Arrizabalaga, P.; Castan, P.; Geoffroy, M.; Laurent, J.-P. *Inorg. Chem.* **1985**, *24*, 3656−3660.
(19) Schmauke, T.; Einar Möller, E.; Roduner, E. *Chem. Commun.* **1998**, 2589−2590.
(20) Reaction of Pt(pop) with 2 equiv of Cr^{2+} in aqueous solution produced a stable species that was tentatively assigned as $Pt(pop)^{6-}$.[40] However, this assignment cannot be correct, because the Cr^{3+}/Cr^{2+} potential (ca. −1.1 V) is more positive than the estimated $E(Pt(pop)^{4-/5-})$ value of −1.8 V. Moreover, the Raman spectrum of the product has a ν(Pt−Pt) band at lower wavenumber than in the Pt(pop) parent.[40]
(21) Heuer, W. B.; Totten, M. D.; Rodman, G. S.; Hebert, E. J.; Tracy, H. J.; Nagle, J. K. *J. Am. Chem. Soc.* **1984**, *106*, 1163−1164.
(22) Lam, Y. C. Ph.D. Dissertation, California Institute of Technology, 2015.
(23) Vlček, A., Jr.; Gray, H. B. *J. Am. Chem. Soc.* **1987**, *109*, 286−287.
(24) Vlček, A., Jr.; Gray, H. B. *Inorg. Chem.* **1987**, *26*, 1997−2001.

DOI: 10.1021/jacs.6b02559
J. Am. Chem. Soc. 2016, 138, 5699−5705

(25) Smith, D. C.; Gray, H. B. In *ACS Symposium Series 394. The Challenge of d and f Electrons*; Salahub, D. R., Zerner, M. C., Eds.; American Chemical Society: Washington, DC, 1989; pp 356−365.
(26) Bridgeman, A. J.; Cavigliasso, G.; Ireland, L. R.; Rothery, J. *J. Chem. Soc., Dalton Trans.* **2001**, 2095−2108.
(27) Hill, M. G.; Sykes, A. G.; Mann, K. R. *Inorg. Chem.* **1993**, *32*, 783−784.
(28) Hunter, B. M.; Villahermosa, R. M.; Exstrom, C. L.; Hill, M. G.; Mann, K. R.; Gray, H. B. *Inorg. Chem.* **2012**, *51*, 6898−6905.
(29) Frisch, M. J.; Trucks, G. W.; Schlegel, H. B.; Scuseria, G. E.; Robb, M. A.; Cheeseman, J. R.; Scalmani, G.; Barone, V.; Mennucci, B.; Petersson, G. A.; Nakatsuji, H.; Caricato, M.; Li, X.; Hratchian, H. P.; Izmaylov, A. F.; Bloino, J.; Zheng, G.; Sonnenberg, J. L.; Hada, M.; Ehara, M.; Toyota, K.; Fukuda, R.; Hasegawa, J.; Ishida, M.; Nakajima, T.; Honda, Y.; Kitao, O.; Nakai, H.; Vreven, T.; Montgomery, J. A., Jr.; Peralta, J. E.; Ogliaro, F.; Bearpark, M.; Heyd, J. J.; Brothers, E.; Kudin, K. N.; Staroverov, V. N.; Kobayashi, R.; Normand, J.; Raghavachari, K.; Rendell, A.; Burant, J. C.; Iyengar, S. S.; Tomasi, J.; Cossi, M.; Rega, N.; Millam, J. M.; Klene, M.; Knox, J. E.; Cross, J. B.; Bakken, V.; Adamo, C.; Jaramillo, J.; Gomperts, R.; Stratmann, R. E.; Yazyev, O.; Austin, A. J.; Cammi, R.; Pomelli, C.; Ochterski, J. W.; Martin, R. L.; Morokuma, K.; Zakrzewski, V. G.; Voth, G. A.; Salvador, P.; Dannenberg, J. J.; Dapprich, S.; Daniels, A. D.; Farkas, O.; Foresman, J. B.; Ortiz, J. V.; Cioslowski, J.; Fox, D. J. *Gaussian 09*, revision C.01; Gaussian, Inc.: Wallingford, CT, 2009.
(30) *ADF2014.06*, SCM, Theoretical Chemistry, Vrije Universiteit, Amsterdam, The Netherlands; http://www.scm.com.
(31) Perdew, J. P.; Burke, K.; Ernzerhof, M. *Phys. Rev. Lett.* **1996**, *77*, 3865−3868.
(32) Adamo, C.; Scuseria, G. E.; Barone, V. *J. Chem. Phys.* **1999**, *111*, 2889−2899.
(33) Raghavachari, K.; Binkley, J. S.; Seeger, R.; Pople, J. A. *J. Chem. Phys.* **1980**, *72*, 650−654.
(34) Andrae, D.; Häussermann, U.; Dolg, M.; Stoll, H.; Preuss, H. *Theor. Chim. Acta* **1990**, *77*, 123−141.
(35) Martin, J. M. L.; Sundermann, A. *J. Chem. Phys.* **2001**, *114*, 3408.
(36) Glendening, E. D.; Badenhoop, J. K.; Reed, A. E.; Carpenter, J. E.; Bohmann, J. A.; Morales, C. M.; Landis, C. R.; Weinhold, F. Theoretical Chemistry Institute, University of Wisconsin, Madison, WI, 2013.
(37) Cossi, M.; Rega, N.; Scalmani, G.; Barone, V. *J. Comput. Chem.* **2003**, *24*, 669−681.
(38) Klamt, A.; Schüürmann, G. *J. Chem. Soc., Perkin Trans. 2* **1993**, 799−805.
(39) van Lenthe, E.; Ehlers, A.; Baerends, E. J. *J. Chem. Phys.* **1999**, *110*, 8943−8953.
(40) Alexander, K. A.; Paul, Stein; Hedden, D. B.; Roundhill, D. M. *Polyhedron* **1983**, *2*, 1389−1392.

DOI: 10.1021/jacs.6b02559
J. Am. Chem. Soc. 2016, 138, 5699−5705